Low-temperature-grown GaAs coplanar waveguide single-photon/two photon absorption autocorrelator

Juan Montoya and Qing Hu
Department of Electrical Engineering and Computer Science and Research Laboratory of Electronics, Massachusetts Institute of Technology, Cambridge, Massachusetts 02139

(Received 16 May 2003; accepted 4 December 2003)

Previously, we have described a low temperature grown GaAs device that uses single-photon absorption to perform a carrier lifetime limited optical autocorrelation of picosecond optical pulses. In this article, we describe how this same device could be used to perform an autocorrelation of femtosecond optical pulses by utilizing two-photon absorption (TPA). Furthermore, we propose how to model and minimize the photocurrent's dependence on the single-photon absorption (SPA) response of the midlevel traps. We find that the SPA response produces a distortion on the TPA autocorrelation signal at low intensities. At large peak intensities ($I_{\text{peak}} \approx 3G$ W cm^{-2}), however, we find that the SPA distortion becomes nearly two orders of magnitude smaller than the TPA signal, and decreases further with increasing intensity. In our discussion, we also describe some of the tradeoffs between using a photoconductor with a large two-photon absorption coefficient and midlevel states as a TPA autocorrelator. © *2004 American Institute of Physics.*
[DOI: 10.1063/1.1644025]

I. INTRODUCTION

Low temperature grown GaAs (LT-GaAs) is a promising material for a variety of ultra-fast optoelectronic applications such as THz imaging, fast analog to digital (A/D) conversion, semiconductor characterization, spectroscopy, and characterization of ultrafast laser pulses. Annealed LT-GaAs contains a variety of desired properties that has contributed to its success, such as its fast recombination time (200 fs), large electron mobility[1,2] ($\mu_e = 3000$ cm^2/Vs), and its large dark resistivity ($\rho \approx 10^6$ Ω cm). In this article, we will discuss the merits of using annealed LT-GaAs as a single-photon absorption (SPA) photoconductive switch, and as a two-photon absorption (TPA) autocorrelator. The SPA mode of operation allows one to characterize the response time of the material, and in addition provides an efficient method to perform a carrier lifetime limited autocorrelation of optical pulsed sources. Furthermore, SPA operation allows for the generation of high frequency electrical signals (≈1 THz) which have immediate applications for high frequency measurement of electronic devices. In this article, we will compare the SPA autocorrelation performance of our LT-GaAs device with a two-photon absorption autocorrelation. The TPA method offers a true autocorrelation of ultrafast pulses that is not limited by the carrier lifetime of the material albeit at the cost of a reduced sensitivity.

II. SINGLE-PHOTON ABSORPTION AUTOCORRELATION

Our single-photon absorption autocorrelation device has been described elsewhere.[3] The device consists of two LT-GaAs photoconductive switches embedded in a coplanar waveguide as illustrated in Fig. 1(a). The dark shading in Fig. 1(a) represents the gold metallic planes and center conductor, while the unshaded region depicts the semi-insulating LT-GaAs. Also shown are two photoconductive gaps embedded within the center conductor of the coplanar waveguide geometry. These photoconductive gaps function as optical switches which effectively provide a conducting path when illuminated and allow current to flow through the gap in the center conductor. In addition, this figure also shows two paths which connect the center conductor to each ground plane. These paths allow us to apply a dc voltage directly across the gap, while measuring the current through the ground plane.

A cross-sectional view of the photoconductive gap is shown in Fig. 1(b). The dimensions used in our coplanar waveguide geometry result in a characteristic impedance of $Z_0 = 35\ \Omega$. Various center conductor gap spacing and geometries were tested, ranging from 2–10 μm for the standard gap devices. The best results were achieved using the interdigitated gap geometry shown in Fig. 1(c). With this geometry, gap spacings as small as 1.8 μm are embedded within a 10×10 μm^2 area.

The current which flows through the center conductor when the gap is illuminated by a pulsed beam and its time delayed replica contains the autocorrelation information of the illuminating pulse. However, if the temporal pulse width is shorter than the response time of the photoconductive switch then the SPA autocorrelation will be limited by the carrier lifetime of the material. This optical impulse response then allows us to characterize the ultrafast dynamics of the photoconductor. When a voltage V_0 is applied across the gap in the center conductor, the high frequency photocurrent which propagates down the transmission line is given by

$$i_{pc}(t) = \frac{V_0}{Z_0 + G(t)^{-1}}, \tag{1}$$

where $G(t)$ is the time varying photoconductance of the gap under illumination. This equation follows from standard

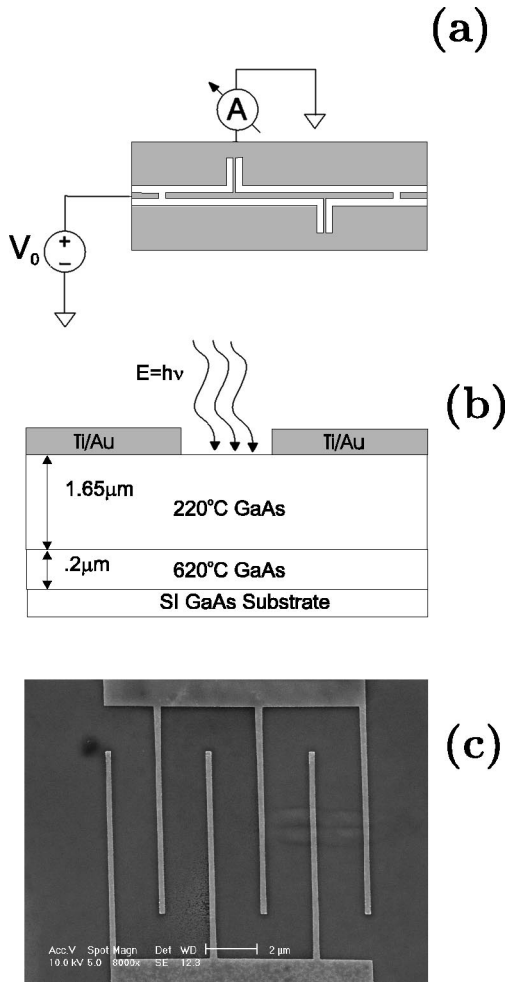

FIG. 1. (a) Top view of the coplanar waveguide (CPW) illustrating the two photoconductive gaps in the center conductor. The shaded area represents the gold region, while the unshaded area represents LT-GaAs. Also shown in (b) is a cross-sectional view of the coplanar waveguide photoconductive gap. The top layer consists of the low-temperature grown molecular-beam epitaxy GaAs, while the 620 °C layer corresponds to normal GaAs. (c) shows the optimal interdigitated finger geometry embedded in the photoconductive gaps of the CPW.

transmission line theory. Instantaneously, the sending end voltage source sees a voltage divider composed of the characteristic impedance Z_0 of the transmission line and the photoconductance $G(t)$. To progress, we need to find a relation between the conductance and the absorbed intensity. For the case in which the incident intensity pulse duration is longer than the response time of LT-GaAs ($\approx$1 ps for large intensities), the conductance may be written as shown in Eq. (2). Here the surface of the photoconductive area is described by a length L, width W, and the thickness of the photoconductive volume is T

$$G(t)=(W/L)\frac{I_0(t)(1-e^{-\alpha T})}{h\nu}q(\mu_e\tau_e+\mu_h\tau_h). \tag{2}$$

We will assume an absorption coefficient $\alpha\approx 16\,000\ \mathrm{cm}^{-1}$ for above the band-gap illumination.[4] The intensity absorbed on the surface is I_0. For book keeping purposes, we will define I_0 to be the difference between the incident intensity I_{in} and the reflected intensity RI_{in} where R is the reflectivity of the LT-GaAs-Air interface ($R\approx 0.3$). Further simplification is made by approximating the conducting surface area to be equal, $W=L$, and by rewriting Eq. (2) in terms of the quantum efficiency η

$$\eta=P_{\mathrm{abs}}/P_{\mathrm{in}}=(1-R)(1-e^{-\alpha T}). \tag{3}$$

It should be noted, however, that for an interdigitated geometry as shown in Fig. 1(c) the approximation $W=L$ is no longer valid. In practice, however, the interdigited geometry has been shown to improve the efficiency over a square gap as a result of the decrease in carrier transit time across the gap.[5] Combining these results we arrive at an expression for the photoconductance

$$G(t)=I_{\mathrm{in}}(t)\frac{\eta q(\mu_e\tau_e+\mu_h\tau_h)}{h\nu}=\gamma I_{\mathrm{in}}(t). \tag{4}$$

In Eq. (4), all the parameters have been lumped into a single constant $\gamma=\eta q(\mu_e\tau_e+\mu_h\tau_h)/h\nu$. An estimate for the above parameters at our operating conditions are $\mu_e=3000\ \mathrm{cm}^2/\mathrm{Vs}$, $\eta=0.7$, $\tau_e=500$ fs, $h\nu=1.5$ eV. The hole contribution is neglected since the hole mobility is much smaller than the electron mobility in LT-GaAs. We now wish to illustrate how we can perform a SPA autocorrelation by measuring the photocurrent of our device. The explicit nonlinear dependence of the photocurrent $i_{\mathrm{pc}}(t)$ with intensity $I_{\mathrm{in}}(t)$ is found by taking the Taylor series expansion of Eq. (1) with respect to $I_{\mathrm{in}}(t)$ in Eq. (4), evaluated at the total peak incident intensity I_p. This result, shown in general terms in Eq. (5) is particularly important because it illustrates that a nonlinearity in intensity I_{in} is introduced by utilizing a voltage divider circuit presented by the characteristic impedance of the transmission line. For instance, without a characteristic impedance ($Z_0=0$), the second derivative of the photocurrent with respect to intensity would be zero.

$$i_{\mathrm{pc}}=i_{\mathrm{pc}}\Big|_{I_p}+\frac{di_{\mathrm{pc}}}{dI_{\mathrm{in}}}\Big|_{I_p}(I_{\mathrm{in}}-I_p)+\frac{d^2i_{\mathrm{pc}}}{2dI_{\mathrm{in}}^2}\Big|_{I_p}(I_{\mathrm{in}}-I_p)^2+\cdots. \tag{5}$$

The intensity-intensity autocorrelation $\langle I_{\mathrm{in}}(t)I_{\mathrm{in}}(t-\tau)\rangle$ of an incident beam $[I_{\mathrm{in}}(t)=I_1(t)+I_2(t-\tau)]$ results from the second order term in the Taylor series expansion, which will produce a mixed product term involving $I_1(t)I_2(t-\tau)$. The other terms result in a constant that does not depend on the time delay τ when averaged over all time. The magnitude of the second order coefficient in the Taylor series expansion determines the sensitivity of the SPA autocorrelator. A typical incident power of 0.1 mW focused on to a 2 μm diameter spot is detectable using this technique.[3]

A. SPA optical impulse response

For the case in which the incident intensity pulse duration is much shorter than the response time of the photoconductive switch $\Delta t\ll\tau_e$, which we will refer to as the optical impulse response, Eq. (2) takes on a slightly modified form. The modified expression may be obtained by using a simplified rate equation as given in Eq. (6)

$$\frac{dn'}{dt}=\alpha I_0(t)/h\nu-n'/\tau_e. \tag{6}$$

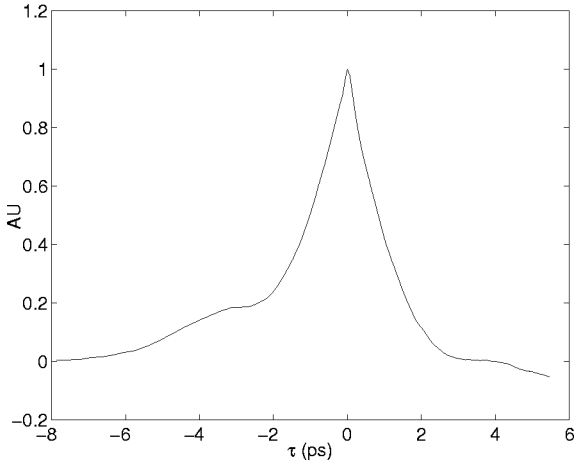

FIG. 2. Carrier lifetime limited autocorrelation performed at an incident wavelength of 850 nm from which a carrier lifetime of $\tau_e = 1.3$ ps is extracted. The incident power used is $P_{\text{avg}} = 15$ mW with bias $= 10$ V.

Equation (6) contains a number of assumptions. First, it assumes that the number of empty traps is not significantly changed throughout the pump duration. Otherwise, the above dynamics would be more complex and would have to account for trap-filling effects. Namely, this implies we are assuming a low-level injection condition on our intensity. In addition, we are assuming uniform illumination, a single level trap recombination process, and neglecting any diffusion current. With these conditions, the carrier concentration becomes

$$n'(t) = \alpha I_\delta / h\nu e^{-t/\tau_e}. \tag{7}$$

In Eq. (7), I_δ is the area of the impulse which approximately equals $I_{\text{peak}}\Delta t_p$ where Δt_p is the pulse duration. For the carrier-lifetime limited impulse response, it follows that Eq. (4) could be modified by substituting $I_{\text{in}}(t) = I_{\text{peak}}(\Delta t_p/\tau_e)e^{-t/\tau_e}$.

A typical autocorrelation denoting the carrier lifetime limited optical impulse response is provided in Fig. 2. This figure shows the exponential shape of the resulting autocorrelation and the carrier lifetime extracted using an exponential fit. The autocorrelation is taken at an average power of 15 mW with a 10 V bias. The 1.3 ps carrier lifetime is found from Fig. 2 by taking a natural logarithm proceeded by a linear fit. Ideally, the autocorrelation signal would be symmetrical. The asymmetry may result from an asymmetric illumination of the gap. Zamdmer measured the carrier lifetime using a pump and probe reflection measurement prior to metalization and found the carrier lifetime to be on the order of 200 fs.[6]

There are several factors which may contribute to an inferred carrier lifetime ($\tau_e = 1.3$ ps), which is of longer duration than the reflection measurement ($\tau_{\text{rm}} = 200$ fs). Namely, the inherent distortion in a coplanar waveguide (even and odd mode distortion), trap filling effects due to a large incident intensity, and parasitic capacitance effects as a result of metalization. The trap filling effects have been analyzed in the literature. It has been reported that as the conduction band fills due to large intensities, the traps saturate and the bottle neck for the carrier lifetime becomes the trap emptying time (hole capture).[7] For large intensities ($I_{\text{peak}} \approx 1\ \text{GW cm}^{-1}$) and short pulse durations ($\Delta t_p = 200$ fs) the carrier concentration predicted by Eq. (7) is on the order of ($n' \approx 10^{18}\ \text{cm}^{-3}$). This is of the same order of magnitude as the number of traps available in LT-GaAs. A broadening of carrier lifetime with increasing intensity has been experimentally observed for our devices.

In this article, we will discuss two electron time constants. The theoretical limit imposed by the number of empty traps is on the order of (200 fs), which agrees with reflection measurements of low intensity. However, for our experiments corresponding to intensities larger than ($I_{\text{peak}} \approx 1\ \text{GW cm}^{-1}$), we find the electron lifetime to be on the order of 1 ps. In Eq. (4), $\tau_e = 500$ fs is used as a compromise between the two cases in order to estimate the photocurrent.

III. TWO-PHOTON ABSORPTION AUTOCORRELATION

A. Background and motivation

Two-photon absorption is inherently a nonlinear process which occurs when an incident photon has energy greater than half the energy gap $E_g/2$ of a semiconductor.[8] In a semiconductor, an electron making a transition from the valence band to the conduction band by this nonlinear process simultaneously absorbs two photons which effectively gives the electron twice the incident photon energy.[9] This property is described by a two-photon absorption coefficient β which determines the strength of this absorption due to the peak incident intensity I. The advent of commercially available ultrafast lasers capable of producing the large peak intensities required for two-photon absorption have spurred research in this area. Recently, two-photon absorption induced changes in conductivity which are nonlinear in intensity have been exploited for commercial ultrafast autocorrelator applications.

Two photon absorption (TPA) has been demonstrated in LT-GaAs by using transmission based pump and probe experiments at wavelengths with photon energies below the energy gap.[9] Recently, other groups have developed two-photon absorption based autocorrelators using different materials and devices such as AlGaAs,[10] ZnSe,[11] and GaN.[12]

Moreover, researchers have recently shown a 451 fs impulse response at 1.55 μm which they attribute to two-photon absorption in LT-GaAs.[13] However, others argue that at that particular wavelength single-photon absorption effects using a two-step mediated process from midlevel traps are likely to be the dominant excitation mechanism for the optical impulse response.[14]

There are several advantages in using two-photon absorption as a method to perform an ultrafast optical autocorrelation. The traditional method of using second harmonic generating crystals usually requires a stringent phase matching and a demanding optical alignment. Moreover, the signal resulting from a second harmonic generation (SHG) crystal is usually much weaker than the fundamental frequency and requires additional components for filtering, sensitive detection using a photomultiplier, and subsequent amplification. Two-photon conductivity (TPC) autocorrelators greatly benefit from their simplicity. By using a TPC scheme, the detec-

tor acts as the nonlinear intensity element thereby reducing the number of components. Moreover, TPC is insensitive to polarization and does not require phase matching.

Another motivating reason to investigate LT-GaAs as a two-photon absorption autocorrelator encompasses the greater spectral range of operation. This is a desired feature for optical communications applications since fiber coupled devices typically operate at a 1.5 μm wavelength where they have minimal dispersion. The previous section described how the LT-GaAs coplanar waveguide (CPW) autocorrelator has already been shown to work for above the band gap light $\lambda < 870$ nm. The TPA regime of operation will allow for it to work with additional photon energies within the midgap to the conduction band. The corresponding supplemental optical wavelength could then range from 900–1550 nm for an upper estimate.

An advantage of an LT-GaAs two-photon absorption autocorrelator over the single photon autocorrelation technique discussed in the last section is that it will result in a true autocorrelation that is not limited by the carrier lifetime of the material. This is a consequence of the nonlinear photoconductance being instantaneous. Since the principles behind the operation are significantly different from the SPA autocorrelation, it may be advantageous to think in terms of the similar case of a second harmonic generating crystal. For a SHG crystal, the nonlinear intensity propagates in free space and a slow detector is then used to detect the square intensity. The analogy with a two-photon conductivity autocorrelator is that one could also imagine a virtual square-intensity I^2 being generated instantaneously and detected simultaneously. Interestingly, both principles of operation are described by a nonlinear polarizability. For a nonlinear medium, the induced polarization may be written as a Taylor series expansion in terms of the incident electric field as

$$P = \chi^{(1)}E + \chi^{(2)}EE + \chi^{(3)}EEE. \tag{8}$$

In Eq. (8), $\chi^{(1)}$ is the first order susceptibility associated with a constant index of refraction n or constant absorption coefficient. The second order susceptibility $\chi^{(2)}$ is associated with second harmonic generation, which is not significant in our material. The third order susceptibility which is responsible for two-photon absorption creates an intensity dependent index of refraction (the real part), and an absorption coefficient which depends linearly on intensity (the imaginary part).[15] In our application we are interested in how $\chi^{(3)}$ relates to a TPA induced change in conductivity of a material since this process forms the basis of operation in our application. The two-photon absorption coefficient β describes the intensity dependent absorption coefficient ($\alpha_{\mathrm{TPA}} = \beta I$). An expression for the two-photon absorption coefficient in terms of the third order susceptibility is given as[16]

$$\beta = \frac{\omega}{\epsilon_0 n^2 c^2}\chi^{(3)\prime}, \tag{9}$$

where $\chi^{(3)\prime}$ is the imaginary component of $\chi^{(3)}$. A more detailed expression relating β to $\chi^{(3)}$ is given by Hutchings and Wherret which takes into account the tensor nature of β.[17] In our analysis, we will treat the two-photon absorption coefficient as a scalar quantity, with a nominal value of $\beta = 35$ cm/GW.[9] We further note that the two-photon absorption coefficient measured for LT-GaAs is greater than that reported for regular GaAs ($\beta = 26$ cm/GW).[9] A simplified expression has been derived for β which involves only three parameters, the band gap E_g of the material, excitation energy $h\nu$, and the index of refraction.[16,18] The general trend of the TPA coefficient has been to decrease with an increase in the energy gap of the material. While this behavior has modeled the differences in the TPA coefficient for large band-gap materials such as GaN, when compared to GaAs, it does not offer any conclusions on the larger TPA coefficient measured in LT-GaAs versus regular GaAs. Without a physical explanation as to why the measured TPA coefficient is 34% larger in LT-GaAs, one must use its reported value cautiously. At any rate, it is assuring to note that the TPA coefficient is predictably larger in LT-GaAs than it is in larger band-gap materials. For example, the values reported in the literature for the TPA coefficient of ZnSe ($E_g = 2.58$ eV), and GaN ($E_g = 3.39$ eV) are $\beta = 6$ cm/GW and $\beta = 17$ cm/GW, respectively.[11,12] It is important to note that for the latter case exciton effects have been suggested to account for the large TPA coefficient at UV excitation. At the midgap infrared wavelength excitation, the TPA coefficient decreases to a value of $\beta = 3$ cm/GW.[12] Incidentally, GaN while attractive for ultraviolet autocorrelations, is not a suitable material for our wavelengths since the midgap wavelength corresponds to 730 nm.

Last, for an application of LT-GaAs as a tetrahertz transceiver, one would like to know whether or not above the band-gap optical excitation ($\lambda < 870$ nm) with large intensity may be used to generate tetrahertz signals. For instance at moderate intensities for band-gap resonant excitation, one would expect a direct transition at the band gap extrema. However, for large peak intensities, TPA effects may become prominent for other locations in k-space which obey the energy selection rule for TPA. Certainly, there is a single-photon absorption cross section which allows for a significant amount of carriers to be generated in the conduction band. Ideally, these carriers could be used to generate high frequency signals as shown in the SPA section. However, as our TPA study suggests, at large intensities TPA generated carriers make a nontrivial contribution to the carrier population and to the photocurrent. These carriers are long lived and studies have shown that the bottleneck to carrier recombination for carriers with such excess energy is through phonon assisted relaxation into the bottom of the conduction band before trap recombination may occur.[2] Our interest in tetrahertz devices further motivated our study of TPA generated carriers. If TPA generated carriers make a nontrivial contribution to the population density, then the implication is that the bandwidth of a tetrahertz device will be significantly lowered at large intensities. However, the question then becomes whether or not this TPA effect may be exploited to perform an optical correlation of ultrashort pulses.

B. Two-photon absorption circuit model

For our time average measurements, it is really the conductance that we are interested in. So we proceed to construct an equation involving the conductance assuming a square illumination area

$$G(t)=G_{\text{dark}}+G_{\text{photo}}(t). \tag{10}$$

We would expect the intensity to decay into the bulk exponentially with a decay constant given by α_t, since the single photon absorption from the traps is greater than the two-photon coefficient. To be more quantitative, the differential equation which describes the intensity absorption depth is written as[19]

$$\frac{dI(x)}{dx}=[-\alpha_t-\beta I(x)]I(x). \tag{11}$$

For our operating conditions, $\beta I(x)$ is an order of magnitude less than the single photon absorption constant. The solution of Eq. (11) indicates that for small β the intensity absorption in the bulk has approximately the same exponential dependence on the absorption coefficient as the case in which only SPA from the traps is present, i.e., $I(x)=I_0e^{-\alpha_t x}$. We may derive an expression for the conductance by modifying Eq. (2). The intensity absorbed on the surface of LT-GaAs in this case is larger by a factor of $(1+\beta/\alpha_t I_0)$. Scaling Eq. (2) by this factor and substituting the trap absorption coefficient α_t for the total absorption coefficient α leads us to an equation for the desired conductance. Note, that in this case the quantum efficiency η decreases for the TPA case since our bulk thickness $T=1.65\ \mu$m is optimized for above the band-gap illumination in which the absorption depth is less than the absorption depth for below the band-gap illumination. For below the band-gap illumination, we expect the single-photon absorption coefficient from the traps[4] ($\alpha_t \approx 4000\ \text{cm}^{-1}$) to be a approximately a factor of four smaller than the above the band-gap case ($\alpha \approx 16\,000\ \text{cm}^{-1}$). This implies that our new absorption depth is ($1/\alpha_t \approx 2.5\ \mu\text{m} > T$). It may appear tempting to increase our bulk thickness, however, this would lead to an increase in the SPA signal which we wish to supress. We will return to this point later in our analysis.

$$G_{\text{photo}}(t)=\eta q(\mu_e+\mu_h)\frac{[\alpha_t+\beta I_{\text{in}}(t)]I_{\text{in}}(t)}{h\nu\alpha_t}$$
$$=\gamma\left[1+\frac{\beta}{\alpha_t}I_{\text{in}}(t)\right]I_{\text{in}}(t)=G_{\text{SPA}}(t)+G_{\text{TPA}}(t). \tag{12}$$

As noted above, the photoconductance has been written explicitly in terms of the trap single-photon absorption and a two-photon interband absorption contribution. Similar expressions have been derived in the literature for other structures.[20] In order to continue our development of the autocorrelator model, a few key points should be observed. The absorbed intensity spectrum contains a combination of high frequency components, and additional low-frequency components which generate an electrical signal. In traditional communications applications, a signal is typically upconverted to a high frequency where the entire signal sees a transmission line with a characteristic impedance Z_0. Since that is not the case here, we will take advantage of using superposition to treat the input as a sum of a high frequency component and a low frequency component in order to solve for the output due to the broad spectrum.

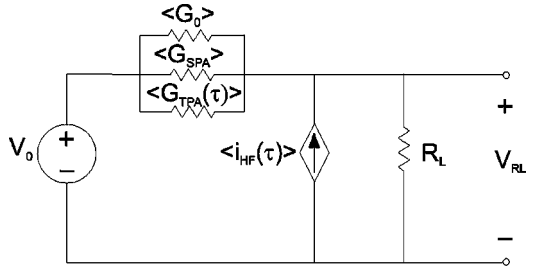

FIG. 3. Circuit to analyze the TPA Measurement. The total time average conductance of the photoconductive switch is $G_t=\langle G_{\text{SPA}}\rangle+\langle G_{\text{TPA}}(\tau)\rangle+\langle G_0\rangle$. The high frequency distortion which results from the single-photon absorption contribution from the traps is represented by the dependent current source $i_{\text{HF}}(\tau)$. The output voltage is measured across a macroscopic load resistor R_L.

In our autocorrelator, we observe that the low frequency component of $G(t)$, essentially the dc component, will not require a characteristic impedance transmission line model (distributed model). Therefore we will model the dc conductance as a lumped element consisting of the time average of the SPA contribution $\langle G_{\text{SPA}}\rangle$, and the background dark conductance $\langle G_0\rangle$. However, the high frequency component of the generated signal will see the characteristic impedance and should be modeled the same as in the SPA section. Essentially, this model allows us to combine the two contributions of SPA from the traps to the total measured signal as shown in Fig. 3. The first contribution $\langle G_{\text{SPA}}\rangle$ does not depend on the delay between the two intensities. The second (high frequency) contribution $\langle i_{\text{HF}}(\tau)\rangle$ is modeled by the second order term in Eq. (5) in the SPA section. Note that in our model, as shown in Fig. 3, we depict the high frequency contribution to the conductance as a voltage dependent current source and the dc component as a lumped element. Explicitly then, we have

$$\langle i_{\text{HF}}(\tau)\rangle=\frac{-V_0\gamma^2Z_0}{(1+Z_0\gamma I_{\text{peak}})^3}\langle I_1(t)I_2(t-\tau)\rangle, \tag{13}$$

for the current source amplitude which may be obtained by using the second order expansion term in Eq. (5). The reason a current source is chosen is due to the observation that changing the macroscopic load (dc resistor R_L) should not change the value of the high frequency current contribution. This result comes from treating the termination as an effective impedance for high frequencies which does not depend on the macroscopic large load resistor R_L. Intuitively, one may imagine that most of the energy of the high frequency signal will radiate or suffer attenuation before reaching the macroscopic load. However, since the bulk thickness is not optimized for below the band gap illumination the current source dependence will be reduced (i.e., $i_{\text{HF}}\propto\eta^2$). In addition, Eq. (13) shows that as the intensity increases the sensitivity of the current source decreases. In summary, our model

illustrates that the single photon absorption contributes a background conductance that is independent of the delay of the two beams and a distortion term that results from the nonlinearity produced by the transmission line. This distortion is modeled as a current source with an amplitude given in Eq. (13). The time average of the two photon absorption conductance

$$\langle G_{\mathrm{TPA}}(\tau)\rangle = \left\langle \frac{\gamma\beta I_{\mathrm{in}}^2(t)}{\alpha_t} \right\rangle \tag{14}$$

contains the autocorrelation signal that we desire, where $I_{\mathrm{in}}(t)=I_1(t)+I_2(t-\tau)$.

We will now provide a comparison of the SPA contribution versus the TPA contribution to the current at an intensity that corresponds to our operating conditions. For a 900 nm Ti:Saphhire source focused down to a $10\times 10\ \mu\mathrm{m}^2$ area with total average incident power of 30 mW, 100 fs pulse duration, and a repetition rate of 100 MHz, we estimate a peak intensity of $I_{\mathrm{peak}}=3\ \mathrm{GW\,cm^{-2}}$. Approximately 30% of the incident power is reflected at the GaAs-air interface ($R=0.3$), which leads to a value of $\eta=0.33$ from Eq. (3) where we used the single-photon absorption coefficient from the traps. Using this value for η along with the material parameters for τ_e and μ_e, we find $\gamma I_{\mathrm{peak}}=1\ \Omega^{-1}$ in the denominator of Eq. (13). This implies that at this intensity, the sensitivity of the SPA current source contribution is largely attenuated by a factor of $(1+Z_0)^3$ in the denominator of Eq. (13), where $Z_0=35\ \Omega$. Comparing the ratio of $\langle G_{\mathrm{TPA}}(0)\rangle V_0/\langle i_{\mathrm{HF}}(0)\rangle$, we find the TPA contribution to the current to be $\approx$70 times larger than the SPA distortion. For larger intensities, the denominator of Eq. (13) further increases leading to greater attenuation of the SPA signal. We also note that the above argument relies on material parameters which have uncertainty due to growth conditions. This may offer an explanation as to why the measured results described in the next section agree with the conventional second harmonic generating crystal technique at a larger average intensity ($P_{\mathrm{avg}}=170$ mW).

While we have provided a qualitative justification for neglecting the SPA signal based on the latter analysis, we will also point out that as the intensity increases we would expect the single-photon absorption contribution to decrease as a result of absorption saturation.

For a dc measurement across the resistor R_L, the output voltage V_{R_L} is given by

$$V_{R_L}=\frac{V_0 G_T R_L}{1+R_L G_T}+\frac{i_{\mathrm{HF}} R_L}{1+R_L G_T}, \tag{15}$$

where G_T is the total time averaged photoconductance. For optimal operating conditions, we would like to have the high-frequency current source contribution minimized and a linear output voltage with respect to the time averaged conductance. This imposes a constraint on our load resistor R_L. Specifically, we will require that $R_L G_T \ll 1$ and $i_{\mathrm{HF}} \ll V_0 G_T$. With this simplification, we could rewrite Eq. (15) as

$$V_{R_L}\approx V_0 G_T R_L = V_0[\langle G_0\rangle+\langle G_{\mathrm{SPA}}\rangle+\langle G_{\mathrm{TPA}}(\tau)\rangle]R_L\,. \tag{16}$$

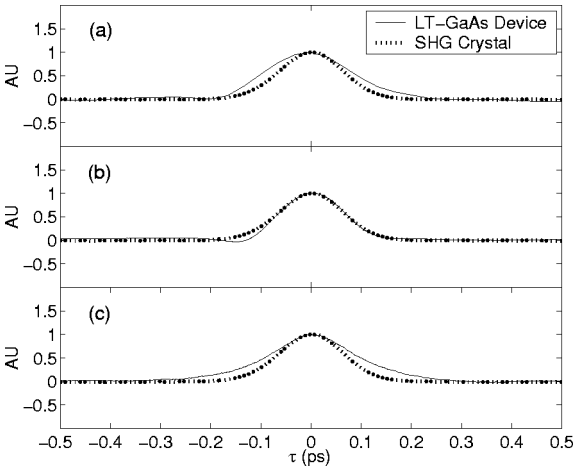

FIG. 4. Two-photon absorption autocorrelation at 900 nm using a speaker with a mounted retroreflector as the delay source τ for (a) $P_{\mathrm{avg}}=30$ mW, bias$=30$ V and (b) $P_{\mathrm{avg}}=170$ mW, bias$=30$ V. Also shown in (c) is a lock-in measurement using a linear delay stage at $P_{\mathrm{avg}}=50$ mW. A lock-in time constant of 1 s was used at a detection frequency of 1.5 kHz. A half-wave plate was used in all measurements to minimize coherence effects. The dashed curve shows a second harmonic generating crystal autocorrelator measurement for comparison. The SHG autocorrelation is measured at 30 mW incident power using a Femtochrome Research Model (FR-103MN) autocorrelator.

The only term in the above equation that depends on the delay (τ) between the two incident beams is the two-photon absorption time averaged conductance $\langle G_{\mathrm{TPA}}(\tau)\rangle$. The remaining terms contribute to a dc offset which may be removed from our measurement.

C. Two-photon absorption measurement

The setup for these experiments consist of an interferometric layout in which the incident beam is split into two beams through a 50/50 beam splitter $[I_{\mathrm{in}}(t)=I_1(t)+I_2(t-\tau)]$. The two beams are focused onto the photoconductive gap in our coplanar waveguide. A half-wave plate is used to achieve orthogonal polarizations of the two beams so that the electric fields do not interfere. If they are to interfere, the consequence will be an undesirable nonlinearity resulting from an additional intensity term $[I_{12}(\tau)]$. This interference term will distort our measured autocorrelation predominantly through a SPA process. In our model, the SPA conductance $\langle G_{\mathrm{SPA}}\rangle$ will now be a function of the delay between the two arms τ and will produce an interferometric e-field correlation distortion on the measured signal.

A portion of an unused beam which is transmitted through one of the beamsplitters in our setup is feed to an Hewlett-Packard Optical Spectrum Analyzer to monitor the central wavelength. The laser is tuned to a central wavelength of 900 nm. This wavelength contains energy that is below the bandgap of LT-GaAs which corresponds to approximately 870 nm. Similar results were observed with incident wavelengths ranging from 900–930 nm.

Two types of measurements are performed. In the first measurement, a speaker with a mounted retroreflector is used as a delay stage. The results of these experiments are shown in Fig. 4(a) for an incident power of $P_{\mathrm{avg}}=30$ mW and in

Fig. 4(b) for an incident power of $P_{avg}=170$ mW. Both measurements are taken with 64 averages by viewing the output voltage V_{RL} of the load resistor on an oscilloscope triggered by the speaker drive signal (20 Hz ac voltage). The output corresponding to a total of 30 mW incident power (15 mW in each arm) shown in Fig. 4(a) is not as good a fit to the SHG crystal measurement as in Fig. 4(b) where the input power is increased to 170 mW. This is in agreement with the behavior our model predicts for an increase in intensity, namely, that the TPA strength increases while the SPA distortion decreases.

In Fig. 4, a purely interferometric electric field-electric field autocorrelation is not observed. If this were the case, one would expect an oscillation centered on the dc background. This would result in a double peaked envelope (above and below the dc background) which is not observed. Another possibility to be considered is that of a superposition of an interferometric electric field autocorrelation and a SPA autocorrelation. If the first order intensity is being absorbed (SPA process), this would give rise to a SPA photoconductance which could be categorized into two types of responses. The high frequency response occurs as a result of the waveguide transmission line. Essentially, the voltage divider presented by the waveguide described in Eq. (1) results in a lifetime limited SPA intensity autocorrelation. The second type of photoconductance response, the dc-average photoconductance, gives rise to the e-field autocorrelation. The combined responses result in a slow decaying tail as in Fig. 2 superposed with a peak at the delay $\tau=0$ where the e-field autocorrelation is maximum which is not observed.

For a second measurement, a lockin amplifier is used in conjunction with a linear delay stage and an optical chopper. The results are displayed in Fig. 4(c). Both beams are chopped at two different frequencies, using the inner and outer blades of a chopper. The average incident power is 50 mW. One drawback of using the lock-in measurement is that the chopper reduces the beam intensity while sampling the beam (i.e., the beam is blocked by the rotating blades). Consequently, a greater average power was not used in order not to damage the device. The measurements were taken using a lock-in time constant of 1 s, and the detection is performed at the sum frequency of $(f_s=1.5\ \text{kHz}=1\ \text{kHz}+500\ \text{Hz})$. The detection at the sum or difference frequency allows us to filter out the signal resulting from the product of the two beam intensities $I_1(t)I_2(t-\tau)$ while blocking out the background terms (i.e., the single photon absorption dc offset). The sum frequency is used to avoid the second harmonic of one of the chop frequencies (500 Hz), and to optimize our detection frequency to avoid $\sim(1/f)$ noise. The linear delay stage used for this measurement allows for a 100 nm step size which provides a measurement independent of the speaker reference frame.

Typically, a plot depicting the photocurrent as a nonlinear function of intensity would suggest a two-photon process. However, in the case of a LT-GaAs device the lifetime limited response also produces a nonlinear dependence of the photocurrent on intensity due to the voltage divider presented by the circuit. A nonlinear dependence of the photocurrent versus intensity has been presented in the literature for similar LT-GaAS devices.[13] However, such a plot is inconclusive as to whether the nonlinearity is the result of the circuit or TPA. We propose that the lifetime limited SPA nonlinearity is much slower than the TPA response, and may therefore be distinguished.

In order to verify our results, we compared our measurements to a commercial autocorrelator produced by Femtochrome Research (Berkeley, CA). Femtochrome's autocorrelator (FR-103MN) uses an $LiIO_3$ second harmonic generating crystal for an intensity–intensity autocorrelation. Their delay stage utilizes a quick scan technique similar to our speaker measurement in terms of speed but instead uses a rotating mirror scheme as the delay source.

Our measurements are performed with an incident power ranging from 30 to 170 mW. At lower intensities, the signal-to-noise ratio is too low to obtain a good measurement. The best measurements occur at the higher incident power levels where we would expect a greater peak intensity and two-photon absorption signal. In addition, as we increase the incident power we would expect the single photon absorption signal from the traps (modeled as a current source) to decrease as a result of two different mechanisms. The first mechanism would be the decrease in the absorption coefficient as a result of band-filling. At these high pump intensities we expect a decrease of the net trap absorption coefficient as a result of the reduced available states in the conduction band and the reduced carriers available in the traps. The second mechanism which reduces the SPA signal follows from the reduced sensitivity in the second order term of the Taylor series expansion of the SPA signal with increasing intensity.[3] Furthermore, at low intensities we did not observe a SPA carrier lifetime limited signal. This is expected since for below the band-gap illumination the absorption coefficient is reduced and our quantum efficiency η is lowered. The single-photon absorption contribution to the distorting signal scales as η^2 while the TPA signal scales with η.

Essentially, this places some design considerations when using LT-GaAs as a TPA autocorrelator. If we design the thickness of the device large enough so that all of the SPA carriers will be absorbed, we will increase the TPA signal. However, this result is obtained at the expense of increasing the SPA distorting signal at low intensities. At large intensities, however, the TPA signal will dominate and the SPA signal will decrease. Decreasing the bulk thickness, essentially lessens the contribution of the SPA distorting signal at low intensities on the one hand, while decreasing the overall gain of the TPA signal on the other.

The autocorrelation signal performed by using TPA resulted in a full width half maximum $\tau_{1/2}$ of 300 fs, which is much narrower than what would be possible with a single-photon absorption carrier lifetime limited autocorrelation. For a lifetime limited autocorrelation, the carrier lifetime (τ_e) may be extracted from the full width half maximum by using $\tau_e=2\ln(2)\tau_{1/2}$. This would result in a carrier lifetime of 208 fs which is much faster than the measured result shown in Fig. 2, particularly at these large intensities where trap filling increases the response time. We should note that the measured SPA signal on this device using above the band-gap illumination resulted in a carrier lifetime of 1.3 ps

as shown in the SPA section. We also note that our signal closely resembles the SHG crystal measurement, with an appropriate $\mathrm{sech}^2(t/\Delta)$ shape which gives us confidence in our results.

D. Conclusions

We have shown that a TPA autocorrelation may be measured with LT-GaAs in spite of the SPA midlevel states. Furthermore, we note that a nonlinear distortion on the time scale of the carrier-lifetime of LT-GaAs may result at low intensity. This distortion will decay exponentially, with typical time constants ranging from 1 to 5 ps. Moreover, our model indicates that the characteristic impedance (Z_0) of our CPW plays an important role in determining the ratio of the two-photon absorption signal to the SPA distortion. When performing a TPA autocorrelation with a material that has midlevel states and a fast recombination time, it is necessary to design the characteristic impedance of the device in a predictable fashion. By using a coplanar waveguide geometry, our model allows us to control the characteristic impedance and minimize the effect of the SPA distortion.

The general trend has been to avoid semiconductors with midgap states and to use some of the larger band-gap materials as TPA autocorrelators. By using a semiconductor with a smaller band-gap, and midgap states, one may succeed in achieving a larger TPA coefficient. This comes at the expense of having short lived carriers which may produce distortions on the time scale of the pulses to be characterized. However, we propose that under certain conditions these distortions may be minimal and predictable. Furthermore, the large two-photon absorption coefficient found in LT-GaAs allows us to design a relatively simple structure with only a few processing steps. A careful analysis remains to be done in comparing regular GaAs to LT-GaAs for the TPA autocorrelator. While LT-GaAs has been reported to have a TPA coefficient 34% larger than regular GaAs,[9] the reported values remain to be both theoretically and experimentally verified. However, by using LT-GaAs we gain the added functionality discussed in the SPA section for above the band-gap illumination.

Moreover, we also reviewed some of the applications and benefits of using our LT-GaAs device in the SPA mode of operation. In the SPA section, we showed that for above the band-gap illumination the device may be used to generate high-frequency signals in an Auston switch configuration. Some of the proposed applications for this high-frequency signal generation include characterization of electronic devices or to perform carrier lifetime limited correlations of picosecond optical pulses. By using a regular GaAs based device, the response time of the semiconductor would be compromised in these applications.

ACKNOWLEDGMENT

We would like to thank Rajeev Ram for providing the fs laser necessary to conduct the TPA experiments, and Song Ho-Cho for his assistance with the SHG measurements.

[1] M. Stellmacher, J. Schnell, D. Adam, and J. Nagle, Appl. Phys. Lett. **74**, 1239 (1999).
[2] M. Beard, G. Turner, and C. Schmuttenmaer, J. Appl. Phys. **90**, 5915 (2001).
[3] S. Verghese, N. Zamdmer, Q. Hu, E. R. Brown, and A. Forster, Appl. Phys. Lett. **69**, 842 (1996).
[4] H. Loka, S. Benjamin, and P. Smith, Opt. Commun. **161**, 232 (1999).
[5] Y. Chen, S. Williamson, T. Brock, F. Smith, and A. Calawa, Appl. Phys. Lett. **59**, 1984 (1991).
[6] N. Zamdmer, Ph.D. Thesis, Massachusetts Institute of Technology, 1999.
[7] A. Lochtefeld, M. Melloch, and E. Harmon, Appl. Phys. Lett. **69**, 1465 (1996).
[8] M. Karkhanehchi, D. Barrow, A. Bryce, C. Hamilton, and J. Marsh, IEEE J. Sel. Top. Quantum Electron. **33**, 933 (1997).
[9] H. Loka, S. Benjamin, and P. W. E. Smith, IEEE J. Sel. Top. Quantum Electron. **34**, 1426 (1998).
[10] M. Karkhanehchi, C. Hamilton, and J. Marsh, IEEE Photonics Technol. Lett. **9**, 645 (1997).
[11] W. Rudolph, M. Bahae, A. Bernstein, and L. Lester, Opt. Lett. **22**, 313 (1997).
[12] C. Sun, J. Liang, and J. Wang, Appl. Phys. Lett. **76**, 439 (2000).
[13] H. Erlig, S. Wang, T. Azfar, A. Udapa, H. R. Fetterman, and D. C. Streit, Electron. Lett. **35**, 173 (1999).
[14] M. Tani, K. Lee, and X. C. Zhang, Appl. Phys. Lett. **77**, 1396 (2000).
[15] C. Rulliere, *Femtosecond Laser Pulses Principles and Experiments* (Springer, New York, 1992).
[16] G. P. Banfi, V. Degiorgio, and D. Fortusini, Opt. Lett. **21**, 1490 (1996).
[17] D. C. Hutchings and B. S. Wherret, Phys. Rev. B **49**, 2418 (1999).
[18] M. Sheik-Bahea, D. Hutchings, and E. Stryland, IEEE J. Quantum Electron. **27**, 1296 (1991).
[19] F. Lacassie, D. Kaplan, T. De Saxce, and P. Pignolet, Eur. Phys. J.: Appl. Phys. **11**, 189 (2000).
[20] F. Laughton, J. Marsh, D. Barrow, and E. Pornoi, IEEE J. Quantum Electron. **30**, 838 (1994).